High-Content Imaging Analysis of the Knockdown Effects of Validated siRNAs and Antisense Oligonucleotides

Jonathan Low, Shuguang Huang, Michele Dowless, Wayne Blosser, Thomas Vincent, Scott Davis, Jeff Hodson, Erich Koller, Eric Marcusson, Kerry Blanchard and Louis Stancato

J Biomol Screen 2007; 12; 775 originally published online May 21, 2007;
DOI: 10.1177/1087057107302675

High-Content Imaging Analysis of the Knockdown Effects of Validated siRNAs and Antisense Oligonucleotides

JONATHAN LOW,[1,*] SHUGUANG HUANG,[2,*] MICHELE DOWLESS,[1] WAYNE BLOSSER,[1] THOMAS VINCENT,[3] SCOTT DAVIS,[3] JEFF HODSON,[3] ERICH KOLLER,[3] ERIC MARCUSSON,[3] KERRY BLANCHARD,[1] and LOUIS STANCATO[1]

High-content imaging (HCI) provides researchers with a powerful tool for understanding cellular processes. Although phenotypic analysis generated through HCI is a potent technique to determine the overall cellular effects of a given treatment, it frequently produces complex data sets requiring extensive interpretation. The authors developed statistical analyses to decrease the time spent to determine the outcome of each HCI assay and to better understand complex phenotypic changes. To test these tools, the authors performed a comparison experiment between 2 types of oligonucleotide-mediated gene silencing (OMGS), antisense oligonucleotides (ASOs), and short, double-stranded RNAs (siRNAs). Although similar in chemical structure, these 2 methods differ in cellular mechanism of action and off-target effects. Using a library of 50 validated ASOs and siRNAs to the same targets, the authors characterized the differential effects of these 2 technologies using a HeLa cell G2-M cell cycle assay. Although knockdown of a variety of targets by ASOs or siRNAs affected the cell cycle profile, few of those targets were affected by both ASOs and siRNAs. Distribution analysis of population changes induced through target knockdown led to the identification of targets that, when inhibited, could affect the G2-M transition in the cell cycle in a statistically significant manner. The distinctly different mechanisms of action of these 2 forms of gene silencing may help define the use of these treatments in both clinical and research environments. (*Journal of Biomolecular Screening* 2007:775-788)

Key words: mitosis, high-content screening, siRNA, antisense oligonucleotide, distribution analysis

INTRODUCTION

OLIGONUCLEOTIDE-MEDIATED GENE SILENCING (OMGS) as both a laboratory tool and as a therapeutic concept has advanced significantly since its initial discovery nearly 30 years ago.[1] Interest in OMGS grew as evidence accumulated that both eukaryotes and prokaryotes use this process to control cellular gene expression as well as to destroy invading viral genomic material. Early OMGS reports focused on antisense oligonucleotides (ASO), which are small, single-stranded oligonucleotides that bind to mRNA through Watson-Crick base-pair hybridization. Hybridization of an ASO with the target mRNA blocks protein synthesis through the activation of RNase H or through steric interference of the ribosome. Initial problems using ASOs in vitro and in vivo included low stability, specificity, solubility, and immune activation.[2,3] Recently, modifications to the ASO structure, such as the addition of a phosphorothioate backbone and 2′-methoxyethyl-modified regions at the 5′ and 3′ ends, increase ASO specificity, affinity, and stability while promoting degradation by RNase H following hybridization with the target mRNA.[4,5] Cancer patients in clinical trials have been treated with ASOs targeted to a variety of gene transcripts including BCL-2, PKC-α, H-Ras, and DNMT-1.[6-9] These same ASOs have also been used in combinatorial chemotherapy in conjunction with antibodies, radiation, or radical prostatectomy. A more recent prostate cancer trial of an ASO targeting the antiapoptotic protein clusterin used laser capture microdissection to harvest prostate cancer cells after radical prostatectomy. The investigators demonstrated up to a 90% knock down of target mRNA and protein, which correlated to drug concentrations in the prostate.[10]

More recently, short, double-stranded RNA (siRNA) was found to suppress gene expression in *Caenorhabditis elegans* and that a mixture of both sense and antisense RNA is up to 10-fold more effective at gene expression knock down than either sense or antisense RNA alone.[11] Double-stranded RNAs are

[1]Cancer Growth and Translational Genetics and [2]Genomic and Molecular Informatics, Eli Lilly and Company, Indianapolis, Indiana.
[3]Oncology, Isis Pharmaceuticals, Carlsbad, California.
[*]These authors contributed equally to this work.

Received Jan 30, 2007, and in revised form Mar 16, 2007. Accepted for publication Apr 1, 2007.

Journal of Biomolecular Screening 12(6); 2007
DOI: 10.1177/1087057107302675

processed in the cell by dimers of Dicer class III RNase, which cleaves the double-stranded RNA into 22-nucleotide siRNA fragments that inhibit gene expression.[12] Once processed by Dicer, the 22-mer siRNAs interact with the RNA-induced silencing complex to identify and destroy target mRNAs.[13] Recently, using tissue culture and mouse xenografts, siRNAs enhanced tumor sensitivity to chemotherapeutic agents in squamous cell carcinoma, osteosarcoma, and mammary carcinoma.[14,15] Although potentially a very powerful therapeutic, siRNAs have not yet been developed fully in the clinic and are currently used in early-stage clinical trials to combat a variety of viral infections where few other treatment options exist.[16,17]

The completion of the human genome sequencing project and the relative ease of synthesis and use of oligonucleotides make OMGS an ideal technology to study loss-of-function phenotypes in the mammalian cells. In addition, OMGS is an ideal tool for testing biological function in a high-throughput setting in conjunction with the emerging technology of high-content imaging (HCI). HCI combines the flexibility of fluorescent microscopy with the power of automated computerized processing and display.[18] Importantly, HCI generates data at both the well and cell level, encouraging analysis of distinct cellular populations found under each experimental condition. As a tool for drug discovery, HCI is an excellent way to capture and analyze complex interactions and perturbations of cellular processes using a wide variety of molecules such as small molecules and interfering RNA.

Recent advances in HCI have made common the collection of multiparametric data sets from high-throughput screening (HTS), but analysis of these data remains a challenge. The few existing statistical methods and models used to validate HCI data across a series of experiments require extensive operator interaction. As HCI data become increasingly complex, analysis of the many parameters determining the activities of a given molecule will require additional tedious analysis of the data by a trained specialist. To ease this burden, we developed and validated informatics tools for the analysis of high-content imaging data and used these tools to demonstrate differences in biological activity between 2 types of OMGS currently being developed as therapeutic agents, siRNAs and ASOs. These informatics tools greatly decrease the amount of time required to analyze HCI data, allow a more robust statistical analysis of cellular populations and subpopulations, and advance HCI data analysis in a data-driven, objective, and statistical fashion.

MATERIALS AND METHODS

Cell culture

HeLa cells (ATCC, Manassas, VA, #CCL-2) were cultured in DMEM (Invitrogen, Carlsbad, CA, #119650084) supplemented with 10% fetal bovine serum (FBS; Invitrogen #1009-148) and 2 mM L-glutamine (Invitrogen #25030-081) and grown at 37 °C with 5% CO_2. For the assays described below, HeLa cells were plated onto poly-D-lysine–coated 96-well dishes (BD, Franklin Lakes, NJ, #356640) at a density of 5000 cells/well in 100 µl of media, as determined by a Coulter Z2 cell and particle counter.

Oligonucleotides

2′-Methoxyethyl (MOE) modified chimeric ASOs were used throughout this study and were synthesized as previously described.[19] siRNA constructs were obtained from Dharmacon (Lafayette, CO) or Ambion (Austin, TX). Between 6 and 50 MOE chimeric ASOs or siRNAs were designed against each target and screened to determine which were most effective at reducing target mRNA as determined by TaqMan real-time reverse transcriptase PCR (RT-PCR) analysis. The top 5 constructs of each type were then transfected at multiple concentrations to determine potency and maximum efficacy of the construct. For the screen, the MOE chimeric ASO or siRNA with the best combination of potency and maximum efficacy was used. For follow-up studies and confirmation, the 2nd-best constructs of each type were also used.

Transfections and compound treatments

HeLa cells were transfected with either ASOs or siRNAs. ASOs, used at a final concentration of 66 nM, were transfected using the Lipofectin system (Invitrogen #18292) according to the manufacturer's specifications. siRNAs, used at a final concentration of 100 nM, were transfected using oligofectamine (Invitrogen #12252) according to the manufacturer's specifications. Transfections were performed using a Multimek-96 automated pipettor (Saigen/Beckmann, Fullerton, CA), and target knock down proceeded for 48 h posttransfection at 37 °C with 5% CO_2. HeLa cells were treated with either nocodazole (Sigma, St. Louis, MO, #74151) or staurosporine (Sigma #S4400) in 0.5% DMSO for 1 or 48 h at 37 °C with 5% CO_2. All transfections and compound treatments were performed in triplicate. OMGS transfections were also repeated and confirmed by an additional operator.

Immunofluorescence

HeLa cells were fixed in 3.7% formaldehyde (Sigma #F-1268) for 20 min at 37 °C with 50 µl of a prewarmed solution containing 11.1% formaldehyde in phosphate-buffered saline (PBS) added directly to the culture media. All following dilutions were performed in PBS at 25 °C. Fixative-containing media were removed, and each well was washed with 100 µl PBS, permeabilized with 50 µl of 0.1% Triton X-100 (Roche, Basel, Switzerland, #92522020) for 15 min at 25 °C, and washed once with 100 µl of 25 °C PBS. Cells were blocked using 1% bovine serum albumin (BSA; Invitrogen #15260-037) for 1 h at 25 °C. Primary antibodies against phosphorylated histone H3 (Upstate Biolabs, Lake Placid, NY, #06-570) and cyclin B1 (BD Pharmingen #554177) were diluted in 1% BSA to a final concentration of 5 µg/ml, and 50 µl of this

mixture was added to each well for 1 h at 25 °C. Each well was washed 3 times with 200 µl of PBS and incubated for 1 h at 25 °C with a solution containing 5 µg/ml goat α-mouse-Alexa-488 (Molecular Probes, Carlsbad, CA, #A-11001), 5 µg/ml goat α-rabbit-Alexa-647 (Molecular Probes #A-21244), and 200 ng/ml Hoechst 33342 (Molecular Probes #21492) in PBS. For some experiments, α-mouse-Alexa-555 (Molecular Probes #21422) and α-mouse-Alexa-647 (Molecular Probes #21236) were used against cyclin B1 (BD Pharmingen #554177). Each well was washed 3 times with 200 µl PBS and stored at 4 °C until analysis.

Fluorescent imaging and analysis

Images of the immunostained wells were captured on a Cellomics Arrayscan Vti using a 10× objective fluorescent detector (Cellomics, Pittsburgh, PA). Subsequent images were analyzed using the Cellomics Target Activation BioApplication. The target activation algorithm identifies objects through Hoescht dye interaction with DNA, and the relative levels and subcellular localization of cyclin B1 and phosphorylated histone H3 were determined through the respective intensities and locations of Alexa-488 and Alexa-647 fluorescence. All fluorescent intensities are displayed as relative fluorescent units. For each cell, along with the intensity from each channel, several nuclear features were also captured including total nuclear area, the ratio of the perimeter of the nucleus compared to its area, and nuclear length-to-width ratio.

Statistical analysis

Histograms were used to investigate the distributional properties of various cell-level phenotypic data. Nonparametric kernel density estimate with Gaussian smoother was used to delineate the distribution profile. For the variable X with the observed values $x_1, x_2, \ldots, x_N$, the Gaussian kernel density estimate is given by

$$\hat{f}_x(x) = \frac{1}{N}\sum_{i=1}^{N}\phi\left(\frac{x - x_i}{\lambda}\right),$$

where the bandwidth λ is determined by Silverman's rule-of-thumb $\lambda = 0.9 \min(\hat{\sigma}, \mathrm{IQR}/1.34)N^{-1/5}$, with $\hat{\sigma}$ being the sample standard deviation and IQR being the sample interquartile range.[20,21] A logarithmic transformation (base 2) was performed to avoid potential skewing of the data due to distribution errors and to stabilize the variance of the subpopulations.[22] Variability plots were then used to examine variation due to cell-to-cell, well-to-well, and plate-to-plate variation. Variance components were calculated to quantify the contribution of variation sources, and *t*-tests were then used to determine the statistical significance of observed distributional differences.

RESULTS

Targeting the cell cycle regulatory machinery with small molecules is a prominent anticancer strategy, which we built on to characterize a variety of phenotypic effects. A significant cell cycle checkpoint is the G2-M transition, which prevents both chromosomal instability and mitotic catastrophe and is the target for numerous anticancer agents. We developed an HCI assay using the Cellomics Arrayscan Vti to identify phenotypic changes resulting from G2-M cell cycle arrest as identified through the expression of cyclin B1 (cyclin B) and phosphorylated histone H3 (pHH3) at the serine-10 position, as well as the amount of DNA as measured through Hoescht staining. Both cyclin B and pHH3 protein levels are temporally and spatially controlled during the cell cycle and are excellent sentinels for the G2-M transition. Specifically, cyclin B expression is required for mammalian cell mitotic entry and accumulates beginning in late S phase, peaks in early mitosis, and is then dramatically reduced during the metaphase/anaphase transition. Histone H3 phosphorylation begins in G2, peaks in mitosis, and is degraded upon cytokinesis. Thus, both proteins have unique and overlapping expression patterns. Hoescht staining of the nuclear material as the cells progressed through the cell cycle was confirmed using traditional flow cytometry and returned results similar to those found in the HCI assay. Cells containing 1 copy of the nuclear material were sorted into a 2N population, and cells containing 2 or more copies of the nuclear material were grouped into a 4N population. The presence or absence of the 2 protein markers, used in conjunction with changes in DNA content and nuclear morphology, allows the determination of cell cycle perturbations.

Before characterizing the effects of ASO and siRNA treatments using this assay, we first determined how several experimental conditions affected the analysis of the HeLa cell cycle. Total DNA content of HeLa cells treated for 48 h with either nocodazole, staurosporine, or an siRNA or ASO to green fluorescent protein (GFP) was measured and visualized using either untransformed plots (**Fig. 1A, C, E, G**) or after a log2 transformation (**Fig. 1B, D, F, H**), in which the fitted curves are the Gaussian kernel density estimates. The plotting of untransformed data consistently led to a skewing of the results, making analysis of even a control population difficult. The skewing of data, associated with whole population measurements, is a common issue between HCI, microarray analysis, and functional magnetic resonance imaging.[22] Logarithmic transformation is a common statistical technique used to stabilize population variation and eliminate skewed distributions found in data generated using technologies measuring large populations.[23] This transformation changes a multiplicative scale into an additive scale and reduces the influence of extreme values such as outliers caused by cell clumps. We chose log2 transformation due to the ease of interpretation, with a 2-fold increase in the raw scale corresponding to a 1 unit difference in the log2-transformed scale. Log2 transformation of the data identified 2 distinct populations of cells where previously these populations were less obvious. An unadjusted plot of total DNA intensity from untreated HeLa cells consisted of 2 poorly defined peaks (**Fig. 1A**); however, transformation of these data generated a plot consisting of 2 well-defined peaks. In

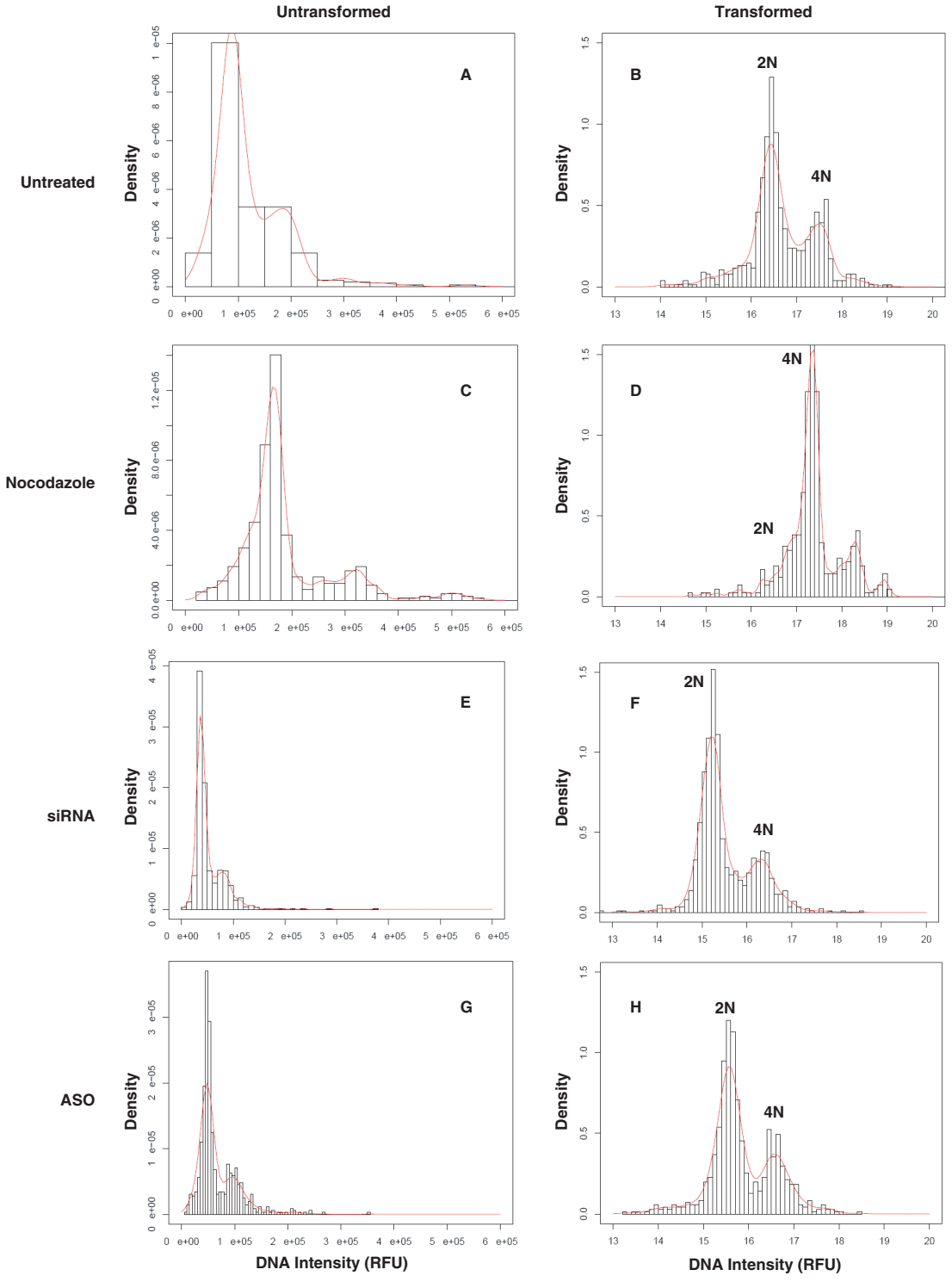

FIG. 1. Comparison between untransformed and log2 transformed analyses. DNA intensity was measured in asynchronous HeLa cells (**A**, **B**), HeLa cells treated with 128 nM nocodazole (**C**, **D**), HeLa cells transfected with 50 nM of a short, double-stranded RNA (siRNA) targeting green fluorescent protein (GFP; **E**, **F**), or HeLa cells transfected with 50 nM of an antisense oligonucleotide (ASO) targeting GFP (**G**, **H**). Data are shown without modification (**A**, **C**, **E**, and **G**) or after log2 transformation (**B**, **D**, **F**, and **H**). All intensities are measured in relative fluorescent units (RFU). 2N and 4N denote the DNA content of the cells under each peak.

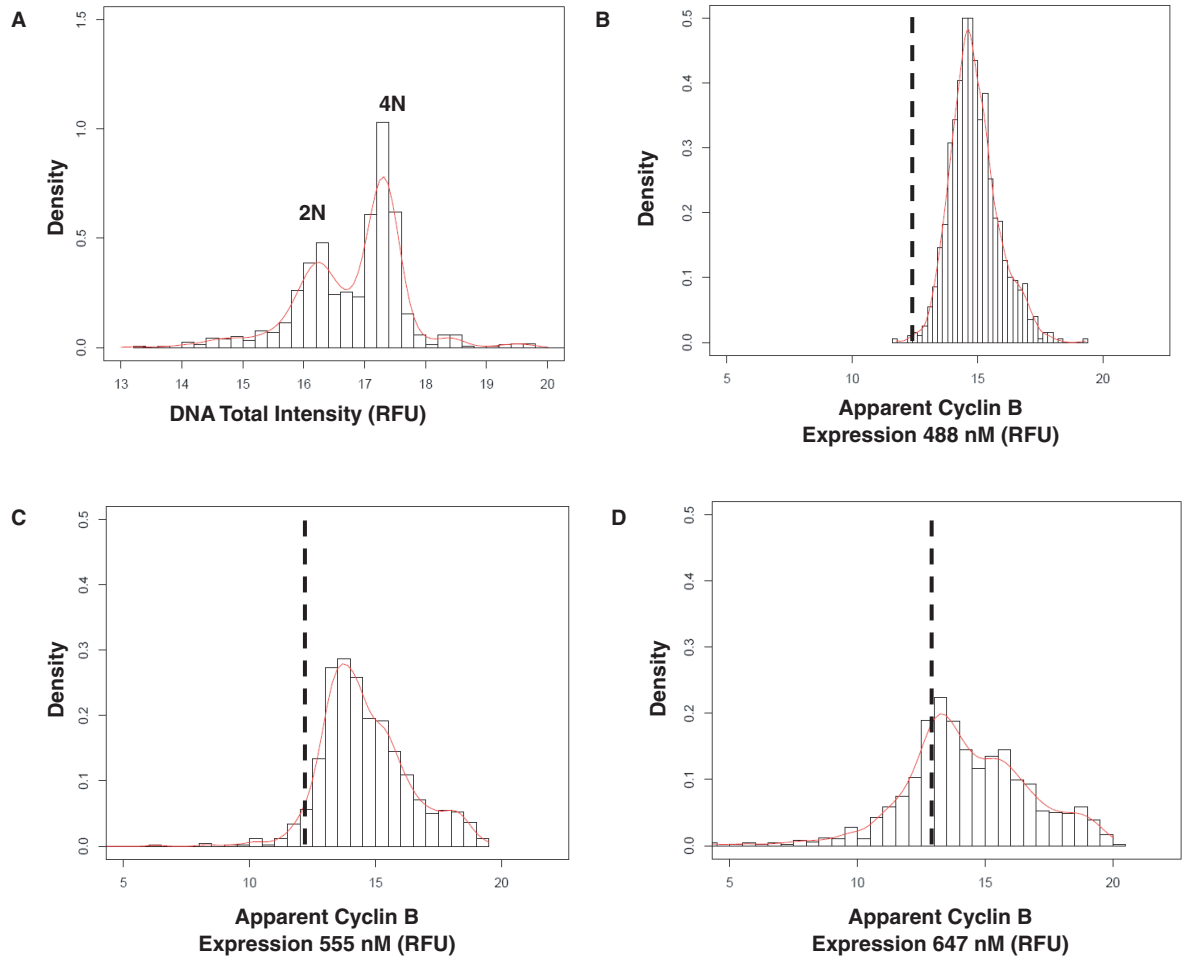

FIG. 2. Effect of compound fluorescence on distribution analysis. DNA intensity was measured from asynchronous HeLa cells treated with 128 nM staurosporine for 48 h and visualized through log2 transformation (**A**). The effects of staurosporine fluorescence on apparent cyclin B expression was measured after incubation of HeLa cells with 20 µM staurosporine for 1 h, followed by fluorescent detection of cyclin B using secondary antibodies excited at wavelengths of 488 nM (**B**), 555 nM (**C**), and 647 nM (**D**). Vertical lines denote the mode of a control population at each wavelength. 2N and 4N denote the DNA content of the cells under each peak.

both cases, the 1st of these peaks is composed of cells with 2N DNA content, and the 2nd smaller peak corresponds to 4N or greater DNA content (**Fig. 1B**).

To confirm the robust nature of subpopulation analysis using a log2 transformation, we tested a variety of cellular perturbations. As expected, the addition of nocodazole, which arrests cells in mitosis through microtubule depolymerization, altered the DNA intensity profile from a 2N major population and a 4N minor population to a 4N major population with 8N and 16N minor populations (**Fig. 1C-D**). Transfection of HeLa cells with an siRNA against GFP produced only minor effects on the population distribution but shifted more cells to a 2N DNA content (**Fig. 1E-F**). Alternatively, transfection with an ASO against GFP slightly increased the 4N or greater population of cells (**Fig. 1G-H**). Interestingly, these population shifts were not observed in the presence of the transfection reagent alone and are therefore likely siRNA or ASO off-target effects.

Treatment of HeLa cells with 128 nM staurosporine also shifted the majority of cells from a 2N to a 4N population, yielding a phenotype similar to that observed following 128 nM nocodazole treatment (**Fig. 2A**). Although the frequently reported fluorescent properties of staurosporine did not significantly alter the DNA content distribution analysis, we wondered how those properties might affect the distribution analysis at other wavelengths and potentially create apparent phenotypic shifts. To further characterize the effects of staurosporine on our distribution analyses, HeLa cells were treated with 20 µM staurosporine for 1 h, fixed, immunostained with α–cyclin B1, and probed for cyclin B expression using 3 secondary antibodies excited at 488 nM, 555 nM, and 647 nM.

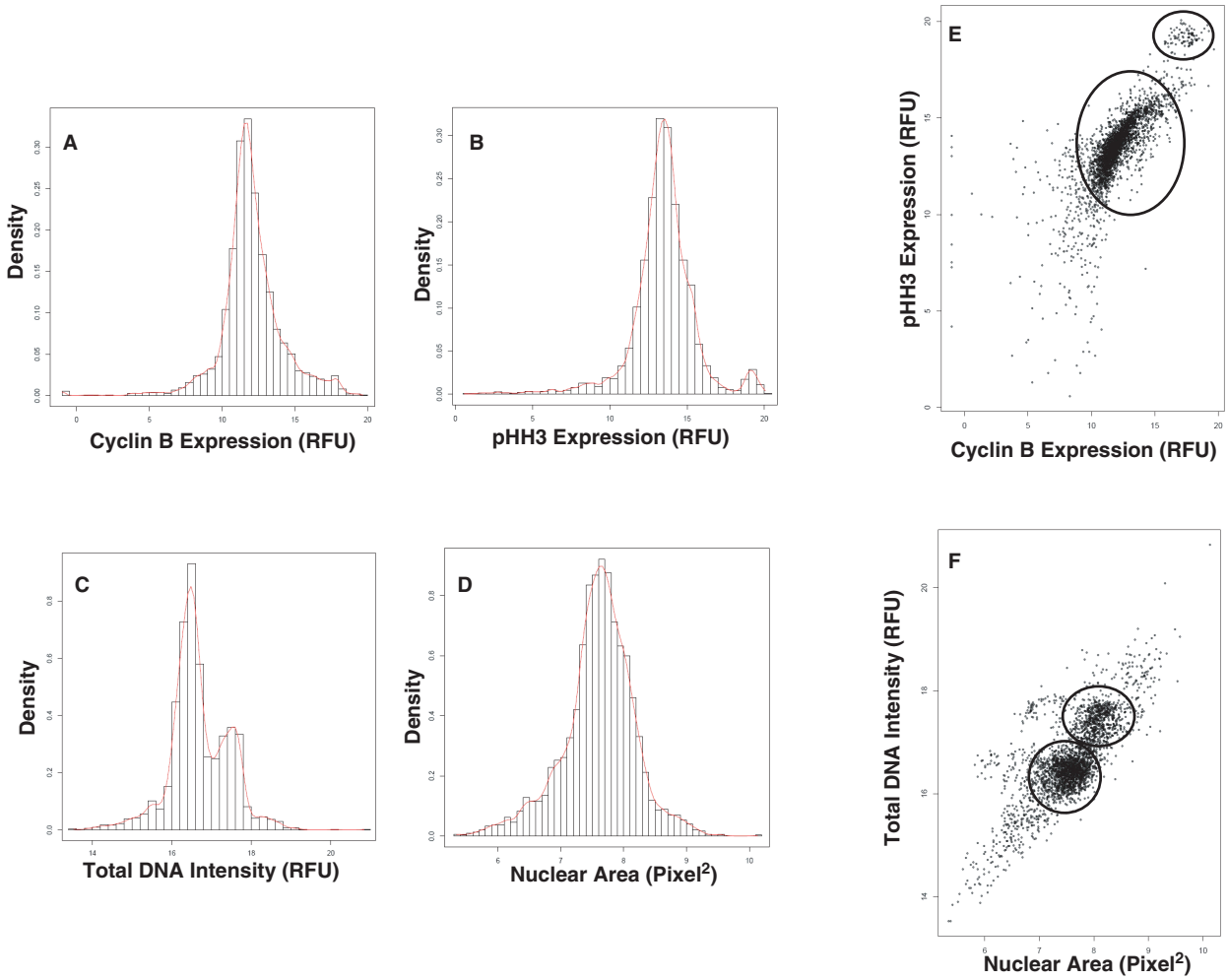

FIG. 3. Multiple high-content parameters distinguish subpopulations within a sample. Distribution analysis of asynchronous HeLa cells was performed using 4 parameters: cyclin B expression (**A**), phosphorylated histone H3 (pHH3) expression (**B**), total DNA intensity (**C**), and nuclear area (**D**). A pairwise scatter plot was then used to compare either cyclin B and pHH3 expression (**E**) or total DNA intensity and nuclear area (**F**).

Compound fluorescence was subsequently measured at each wavelength. The short incubation time with staurosporine allows the HeLa cells to take up the compound without effects on cyclin B expression. Measurement of cyclin B expression in cells following fluorescent excitation at 488 nM determined that there was a nearly 5-fold right shift in the cyclin B peak due to staurosporine fluorescence at this wavelength (**Fig. 2B**). A similar but diminished effect was noted on cells excited with 555 nM light (**Fig. 2C**). Finally, when cyclin B expression was quantified after excitation at 647 nM, we found that the distribution of the staurosporine-treated cells was similar to the distribution of those treated with media alone, indicating no compound fluorescence at this excitation wavelength (**Fig. 2D**). Although the fluorescent properties of compounds such as staurosporine affect the distribution analysis, these same properties also allow visualization and even quantitation of cellular compound uptake.

Examination of HCI data based on information from a single attribute significantly eases the analysis of large screening data sets; however, combining multiple attributes often uncovers previously unidentified populations. The addition of a 2nd attribute in the analysis also creates a more robust statistical confirmation of populations originally defined by a lone attribute. Four phenotypic markers were assessed from a population of asynchronous HeLa cells: cyclin B1 expression (**Fig. 3A**), pHH3 expression (**Fig. 3B**), total DNA intensity (**Fig. 3C**), and nuclear area (**Fig. 3D**). Phenotypic measurements were grouped using pairwise scatter plots by comparing either cyclin B and pHH3 (**Fig. 3E**) or total DNA intensity and nuclear area (**Fig. 3F**). The plot comparing cyclin B and pHH3 expression defined 2 distinct

populations of cells with 1 population of cells expressing high levels of both cyclin B and pHH3, likely a mitotic population, and another population expressing reduced pHH3 and varying levels of cyclin B. The use of 2 attributes together robustly defined these subpopulations, whereas either of the attributes alone led to 2 poorly distinguished clusters or even a single group of cells. Similar patterns emerged upon examination of nuclear area and total DNA intensity (**Fig. 3F**). Although populations were discerned using only total DNA intensity, the addition of a nuclear area measurement further characterized the 2 discrete populations that were otherwise less clearly defined. Pairwise Pearson correlations between the attributes used above demonstrate a strong correlation between nuclear area and total DNA intensity ($\rho = 0.802$), indicating that larger cells generally contain more DNA and moderate correlation between cyclin B and pHH3 expression ($\rho = 0.573$), signifying that although there is an overlap in the expression of these 2 molecules during G2 and mitosis, they have distinct expression patterns.

Although HCI produces large amounts of data in a relatively rapid fashion, efficient screening requires defined guidelines to determine a relevant, but not excessive, population size because of the time necessary to obtain the data from each treatment as well as data storage requirements. As high-content imaging becomes more commonly used for screening, these standards may then be used to validate data from a wide range of experiments. We determined the number of data points required under each condition to ensure the detection of a statistically stable sampling of a given population. HCI data characterizing total DNA intensity, nuclear area, cyclin B, and pHH3 expression were obtained from 3 replicate 96-well plates of asynchronous HeLa cells. We captured 25 fields from each well, yielding a total sampling of 7200 fields corresponding to 462,993 cells with an average of 64 cells captured in each field. These data were then pooled to determine variation at the cell, field, and plate level (**Table 1**). Not surprisingly, the major contributor of variation in this sampling occurred between the cells themselves and accounted for more than 95% of the variation detected in each of the 4 parameters measured.

To determine the variation of cyclin B expression found between fields, we plotted the average of the total intensity of cyclin B for each of the 25 fields in each of 12 wells (**Fig. 4A**). The range of the mean values determined in each of these wells (e.g., 11.6-13.1 in well 1) is much smaller than the range of cyclin B expression across the entire population, which ranges from 5 to 20 (**Fig. 4B**). The biological variance from cell to cell for cyclin B was 2.71 (**Table 1**), so we expected the field-to-field variation to be $2.71/\sqrt{64} \approx 0.34$, with 64 equal to the number of expected cells in each field. If the data are assumed to follow a normal distribution, the range of cyclin B expression in these cells was expected to cover 6 standard deviations. The standard deviation was thus estimated by dividing the range of 1 well by 6 standard deviations, (13.1-11.6)/6, generating a value of 0.25, illustrating that field-to-field variation was similar to that expected from a random distribution of biological variations. **Table 1** shows that the variation between fields due to differences other than biological is 0.0312, or only 12% of the total field-to-field variation. We conclude that variation due to field measurements was minor compared to biological variation and, in turn, that the fields were a simple random sampling of the cell population and therefore representative of the entire well population.

Table 1. Analysis of Variance Components for Multiple Cell Parameters

Parameter	*Source*	*Variance*	*% of Total*
Total cyclin B	Plate	0.0119	0.431
	Well (plate)	0.0117	0.422
	Field (plate, well)	0.0312	1.13
	Cell	2.7077	98.017
Total pHH3	Plate	0.0863	1.329
	Well (plate)	0.0561	0.863
	Field (plate, well)	0.1688	2.599
	Cell	6.1854	95.209
Total DNA	Plate	0.0005	0.07
	Well (plate)	0.0065	0.939
	Field (plate, well)	0.0124	1.754
	Cell	0.6872	97.238
Area	Plate	0.0005	0.107
	Well (plate)	0.0005	0.12
	Field (plate, well)	0.0081	1.853
	Cell	0.4304	97.92

pHH3 = phosphorylated histone H3. Breakdown of variance components in a hierarchy of variation importance from highest to lowest: cell, field, well, plate. In the table, A (B) denotes the source of variation due to factor A, which is nested in factor B.

Once we established that field-to-field variation had little effect on HCI results, we assessed differences between replicate plates. We plotted the average of total cyclin B (**Fig. 4C**) and pHH3 (**Fig. 4D**) expression detected in each field for each of the 2400 fields on each of the 3 plates. Although the plates were intended to be biological replicates, there was indeed a statistically significant variation between the plates when comparing the average total intensity of cyclin B or pHH3, with a *p*-value of 1.79×10^{-4} for cyclin B and 1.21×10^{-7} for pHH3. This variability is likely due to systematic differences in plate manufacturing, cell incubation, or staining procedure. Fortunately, minor plate-to-plate variation, responsible for less than 0.5% of all variation in cyclin B and 1.35% pHH3 expression (**Table 1**), was a negligible contributor to the overall experimental variation.

Finally, we determined the minimum number of cells that must be counted to obtain a statistically reliable sampling of the subpopulations in each well. A population of cells was obtained from 25 fields in 1 well, and HCI attributes measuring total DNA intensity, cyclin B and pHH3 expression, length-to-width ratio, and perimeter-to-area ratio were used to characterize the

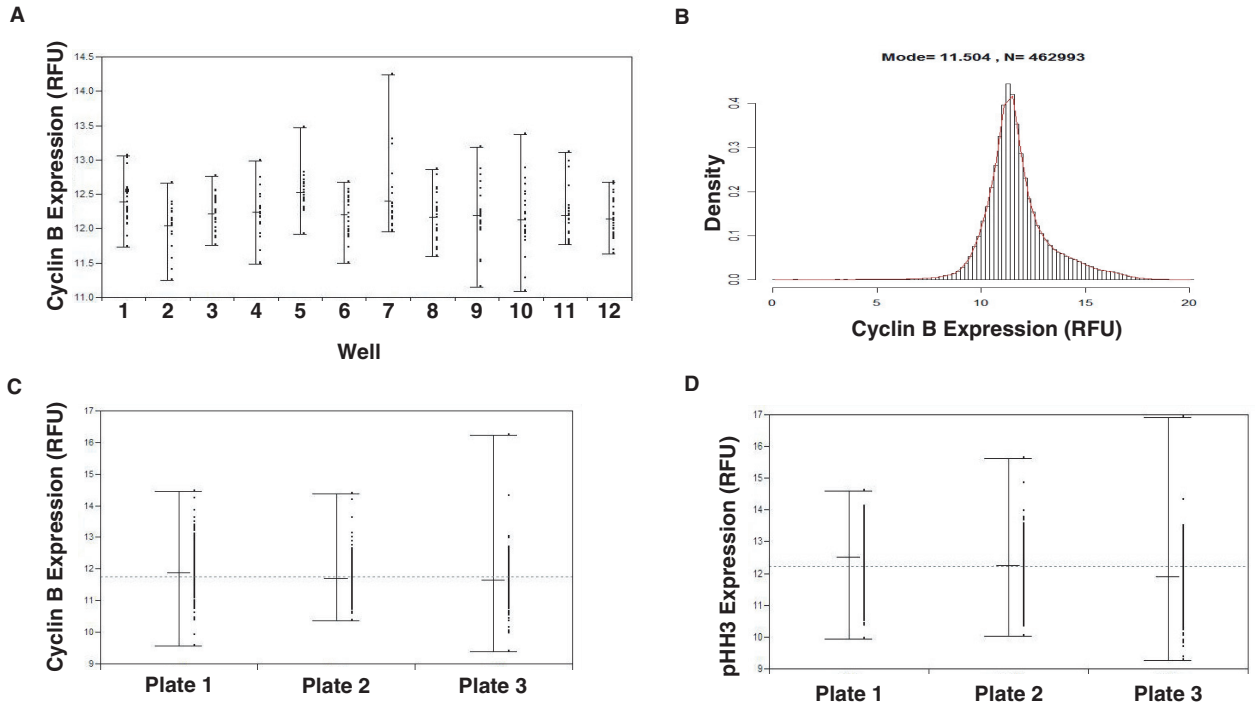

FIG. 4. Variance of data from three 96-well plates. The average total intensity of cyclin B expression was measured for each field in a total of 12 wells (**A**) or for the entire population of 7200 fields (**B**). The average total intensity of cyclin B (**C**) and phosphorylated histone H3 (pHH3; **D**) expression in each field was measured from 3 replicate plates of asynchronous HeLa cells. For each plate, the minimum, maximum, and mean are denoted, with the dotted line indicating the grand mean of the combined data of all 3 plates. All data are log2 transformed.

population. Experimental populations were generated from the total population by gradually decreasing the number of fields analyzed to determine how many fields could be removed before the data set became unstable and significantly differed from the total population. For each decrease in field number, 400 random samplings were performed, and *t*-tests were used to determine statistically significant differences between the experimental population and the control population of all 25 fields. From this analysis, we established that at least 10 fields, corresponding to 600 cells, must be counted under each condition to maintain a 95% confidence limit that a sampled population does not significantly differ from the control population. This result defined the number of cells that must be counted under each condition in an RNAi screen to obtain a statistically significant sampling of the population.

Despite numerous reports on the use of ASOs or siRNAs, few have focused on the different effects that these 2 techniques have on the target cell or have been limited to a single target mRNA.[24] We assessed the potential of 50 validated ASOs and siRNAs to induce cell cycle changes using the HeLa cell G2-M HCI assay, capturing nuclear attributes as well as pHH3 and cyclin B1 expression. The selected targets were largely kinases likely to play a role in cell cycle progression, intracellular signaling, or in DNA replication and repair. To validate the knockdown potential of the reagents, multiple siRNAs and ASOs were transfected into HeLa cells, RNA was extracted, and quantitative real-time RT-PCR was performed to determine expression levels of the targeted genes. We selected the construct demonstrating the greatest knockdown for each target, with a minimum knockdown of 70% expression relative to the transfected control cells for ASOs or 65% expression for siRNAs (**Table 2**). Knockdown of protein expression was confirmed by immunoblot for a number of targets (data not shown).

HeLa cells were transfected in triplicate with individual oligonucleotides; 48 h later, they were immunostained for cyclin B and pHH3 expression and detected with a Cellomics Arrayscan Vti using the Target Activation Bioapplication. Initial data analysis was performed by establishing a basal level of total DNA intensity as well as cyclin B and pHH3 expression equal to that of the trimmed mean of all the experimental samples. As it is well known that ASOs and siRNAs induce sequence-specific off-target effects, using the trimmed mean as a baseline diminishes the potential that off-target effects from a small set of sequences will affect the final average from the

Table 2. Validation of siRNA and ASO Constructs

	% Expression Remaining	
Target	*ASO (66 nM)*	*siRNA (100 nM)*
1	6	2
2	17	11
3	12	11
4	9	12
5	9	12
6	10	13
7	9	13
8	13	13
9	9	14
10	10	15
11	7	15
12	9	16
13	4	16
14	7	16
15	9	17
16	15	17
17	13	18
18	12	18
19	27	18
20	20	18
21	12	19
22	8	20
23	6	20
24	9	20
25	24	20
26	20	20
27	1	21
28	20	21
29	8	21
30	29	22
31	5	22
32	25	23
33	13	23
34	19	23
35	10	23
36	12	24
37	7	24
38	9	24
39	4	25
40	14	30
41	19	25
42	16	26
43	16	26
44	19	32
45	21	27
46	21	2
47	26	32
48	16	29
49	23	31
50	25	33

Antisense oligonucleotides (ASOs; 66 nM) and short, double-stranded RNAs (siRNAs; 100 nM) were transfected into HeLa cells. RNA extracted from these transfections was analyzed through quantitative real-time reverse transcriptase PCR with the percentage remaining expression noted in the % Expression column. Minimum acceptable expression was determined to be 30% for ASOs and 35% for siRNAs.

tested molecules. Changes in cyclin B or pHH3 expression and total DNA intensity induced through siRNA (**Fig. 5A**) or ASO (**Fig. 5B**) treatment were then compared to their respective population's trimmed mean values, with a value greater than 3 standard deviations from the trimmed mean (corresponding to a 95% confidence limit) considered significant. Knockdown of a large number of both siRNA and ASO targets caused an increase in 1 or more cell cycle parameters, but less frequently was a significant difference detected in all 3 markers simultaneously. Results for the 2 types of OMGS were also quite dissimilar, with few siRNAs and ASOs to the same target leading to a G2-M arrest phenotype (**Table 3**). When siRNAs targeting MAP4K5, AKT3, and AURKA were used to knock down their respective targets, we detected significantly higher total DNA intensity as well as increased expression of both cyclin B and pHH3, suggestive of a G2-M arrest. Although knockdown of a number of targets using ASOs increased 1 or more G2-M assay markers, surprisingly, only an ASO targeting AKT3 led to an increase in all 3 chosen attributes. Unfortunately, because of the nature of transfection, the analysis of data at the well level includes both treated and untreated cells, which often makes discerning the effects of a target molecule on a treated population difficult to interpret.

Although total DNA intensity, cyclin B, and pHH3 are relatively robust markers for cell cycle arrest at the G2-M transition, increases in these markers may be masked by the presence of a larger untransfected population. Although in some cases, the population of treated cells demonstrated a phenotype detectable using standard analysis techniques, we suspected that several additional treatments resulted in cell cycle arrest or delay, which may require a more sensitive analysis. We therefore performed distribution analysis on each of the triplicate samples to identify the differential treatment effects on cellular subpopulations in each well. Using DNA content to define the subpopulations, we determined the percentage of cells demonstrating a shift to 4N DNA content as demonstrated by the knockdown of AKT3 (**Fig. 6A**). As previously indicated, the percentage of cells with 4N DNA content was compared to the trimmed mean of all the treatments, with a difference of greater than 3 standard deviations considered significant (**Fig. 6B**). This analysis identified additional siRNAs and ASOs that caused DNA content shifts in both the 2N and 4N directions. siRNAs to the targets MAP4K5, AKT3, PLK2, TLK1, AURKA, AKT2, and MAPK6 all resulted in a population of cells shifted to 4N DNA content, whereas knockdown of MAPKAPK3 or MAPK1 resulted in an increased 2N DNA content population. Treatment of HeLa cells with ASOs targeting MEK1, BUB1, CDK2, AKT3, CSK, MAP3K6, and PDPK1 all resulted in increased 4N DNA content, whereas MAPKAPK2, CHEK1, or a single proprietary target knockdown resulted in a shift to a greater percentage of cells with 2N DNA content. Although several siRNAs and ASOs caused cell cycle

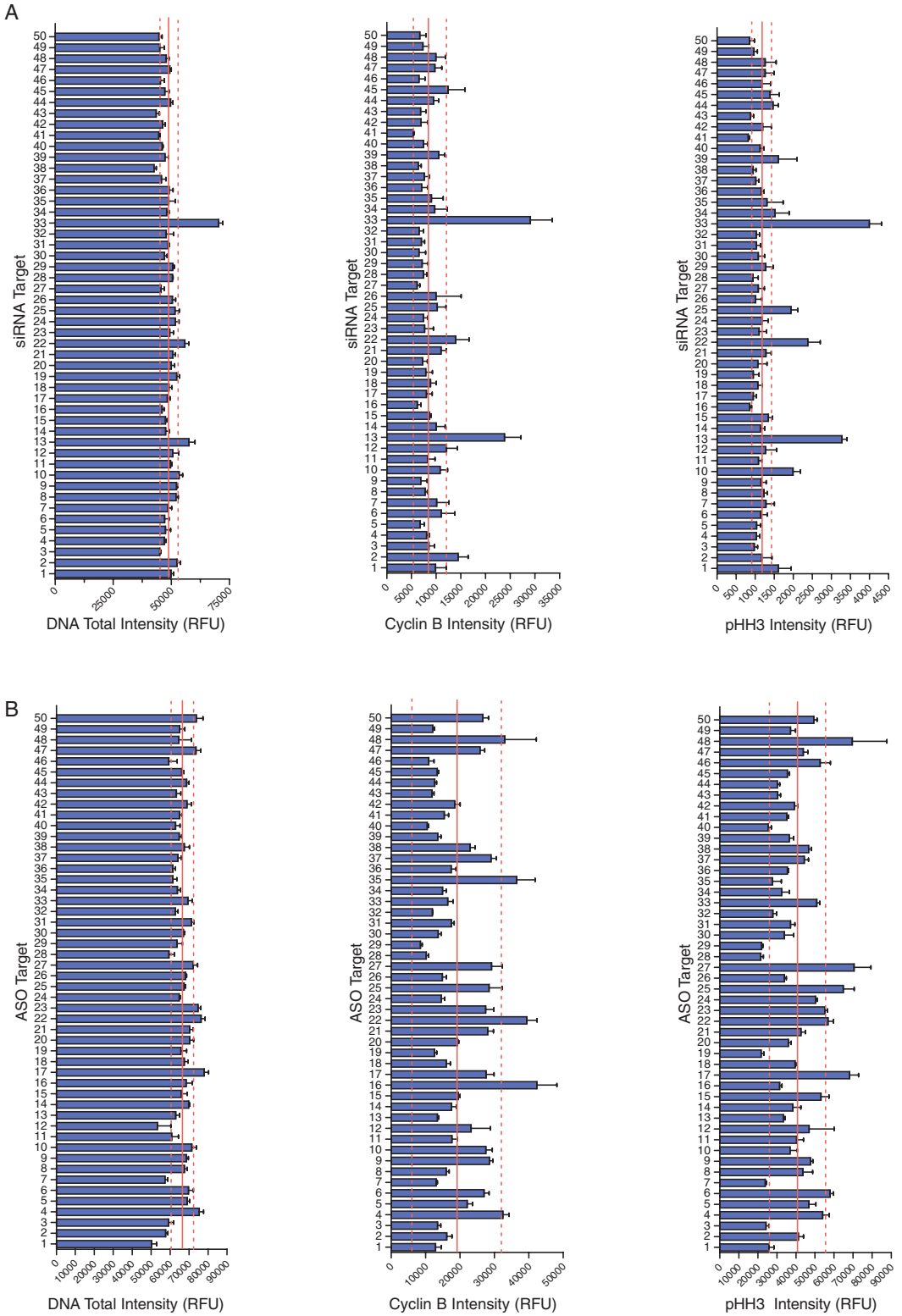

FIG. 5. Effects of short, double-stranded RNA (siRNA) or antisense oligonucleotide (ASO) treatment on cyclin B expression, phosphorylated histone H3 (pHH3) expression, and total DNA intensity. HeLa cells transfected with molecules against the listed targets were probed for the expression of cyclin B, pHH3, and total DNA intensity after knockdown by siRNA (**A**) or ASO (**B**). Listed values are the average of 3 replicates. The solid line represents the trimmed mean, and each dashed line denotes 3 standard deviations from the trimmed mean.

Table 3. Significant Changes in Cyclin B Expression, pHH3 Expression, or Total DNA Intensity from ASO or siRNA Target Knockdown

	siRNA				*ASO*		
Target	*Total DNA*	*Cyclin B*	*pHH3*	*Target*	*Total DNA*	*Cyclin B*	*pHH3*
AKT2			up	AKT3	Up	Up	Up
AKT3	Up	Up	Up	ARAF			Down
AURKA	Up	Up	Up	CDK2	Up		Up
BUB1	Up		Up	CDK4	Down		
CDK4	Up	Up		CDK6	Down		Down
CDK6	Down			CHEK1	Down		
CDK7			Up	CSK	Up		Up
CHEK2			Up	FRAP1		Up	
MAPK6		Up		JAK1			Up
MAP2K6		Up		MAPK1			Up
MAP3K1	Down			MAP2K6	Down		
MAP3K3	Down		Down	MAP3K6	Up		
MAP3K7	Up			MAP3K7			Down
MAP4K5	Up	Up	Up	MAPKAPK2	Down		
MAPKAPK2			Up	MAPKAPK3	Down		Down
NEK2	Down			MEK1	Up		
PAK1	Up			PIK3CA		Up	Up
PDPK1	Down		Down	PKPK1	Up		
PIK3CB	Down		Down	PLK2			Up
PLK2			Up	PT	Down		Down
ROCK1			Down	ROCK1		Up	

pHH3 = phosphorylated histone H3; ASO = antisense oligonucleotide; siRNA = short, double-stranded RNA; PT = proprietary target. Listed targets increased (up) or decreased (down) phosphorylated histone H3 (pHH3) expression, cyclin B expression, or DNA intensity by more than 3 standard deviations from the trimmed mean.

arrest or delay, knockdown of AKT3 was the only target to lead to arrest in both systems.

More recent work in our laboratory compared the results from a cell proliferation assay in 4 cancer cell lines to our earlier HCI data. HeLa, U87MG, Calu6, and HCT116 cells were transfected with the siRNAs and ASOs used in our initial screen to determine effects on cell proliferation. Interestingly, although there was a variation between the siRNAs and ASOs that led to inhibition of cell proliferation in each of the 3 cell lines, the siRNAs and ASOs that led to knockdown in 1 cell line generally led to knockdown in all the tested lines. Differential specificity and effectiveness between siRNAs and ASOs suggests that there may be an important place for both of these technologies in the clinic for the treatment of tumors with differing phenotypes.

DISCUSSION

Although HCI is most frequently used for the rapid quantitation of cellular protein expression, fluorescent detection of cellular markers is neither a novel technique nor the only useful feature of this technology. Along with the quantitation of the desired markers, HCI also characterizes the morphology of each cell, nucleus, or organelle of interest, generating a far more complete picture of how a given treatment affects each cell. In addition to the efficiency and productivity associated with assessing simultaneous multiple individual cellular parameters, HCI links these parameters to create an unparalleled view of cellular processes. A major advance is the movement away from total well-based readouts, in which subtle changes to cellular parameters are often masked, toward true subpopulation analysis, which resolves the variety of populations that comprise the total population. Of course, HCI-based readouts yield large, complicated data sets necessitating new approaches to data analysis to fully exploit this advantage.

To address the need for robust HCI data handling and statistical analysis tools, we developed several strategies to simplify examination of HCI data. Single-parameter distribution analysis, although a relatively simple tool, illustrates how automated statistical analysis greatly simplifies the investigation of large data sets. Multiparameter distribution analysis reveals that further processing of HCI data may define cellular subpopulations not found when monitoring a single parameter. The continued refinement of HCI analysis tools to support additional parameters in a single analysis will further identify and characterize distinct subpopulations previously concealed in complex phenotypic data sets. We are currently developing additional statistical methods and validated markers to simplify HCI data interpretation into a

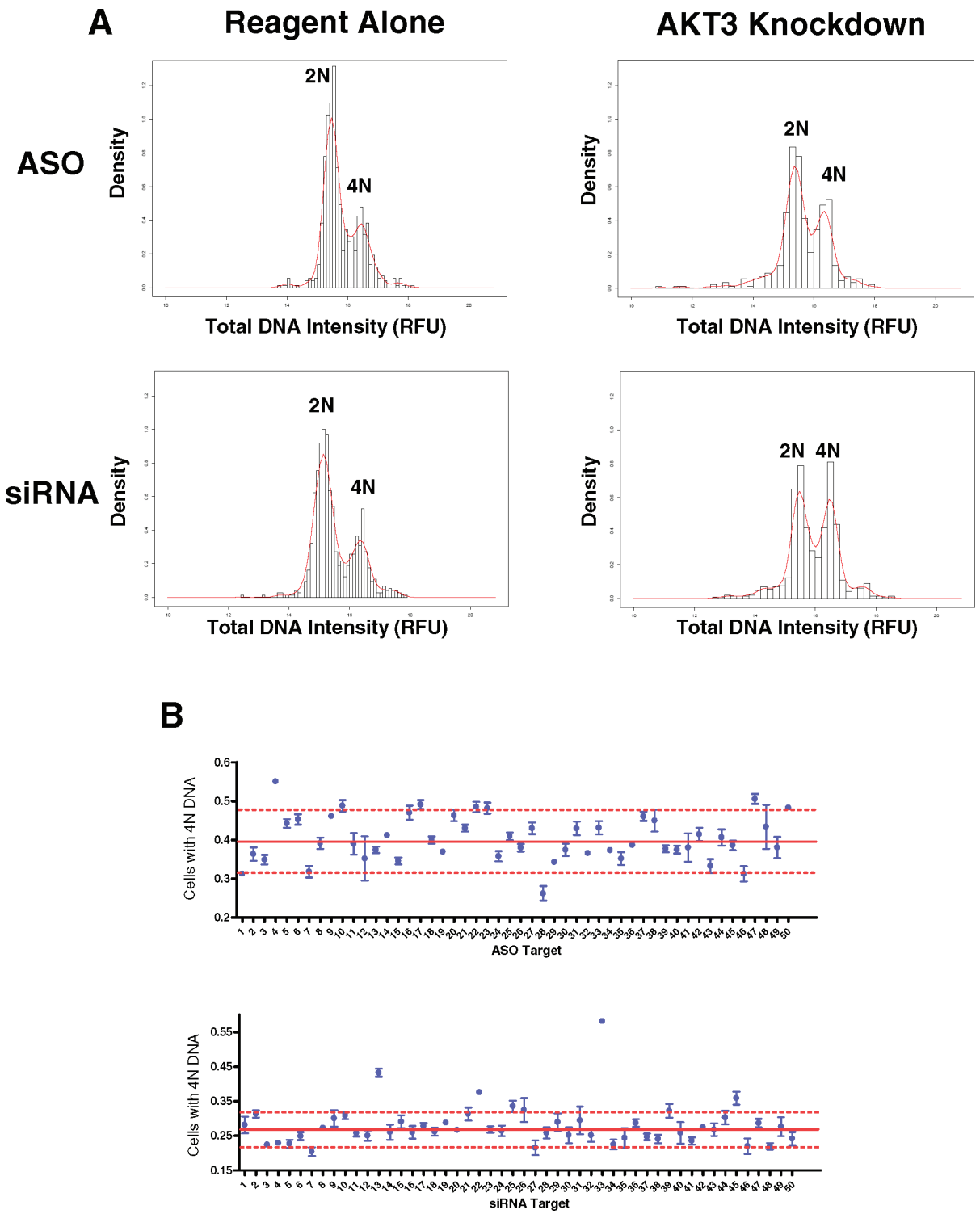

FIG. 6. Subpopulation shifts due to antisense oligonucleotide (ASO) or short, double-stranded RNA (siRNA) treatment. Distribution analysis of total DNA intensity was performed following knockdown of each target. The DNA content of each cell was determined, and cells grouped into 2N and 4N populations with control distributions are shown after incubation with media alone. Shifts away from the control distribution are demonstrated by ASO or siRNA knockdown of AKT3 (**A**). DNA content changes were determined for each RNAi treatment and compared to the trimmed mean (solid line) of all experimental samples (**B**). Knockdown of experimental targets generating population shifts greater than 3 standard deviations (dashed lines) from the trim mean were considered significant. 2N and 4N denote the DNA content of the cells under each peak.

format that can quickly and easily be examined to identify distinct biological effects that would otherwise be masked.

When analyzing data from assays in which only a subpopulation of cells is affected because of transfection efficiency, it is crucial to define appropriate markers and identification criteria to determine treatment effects. In this assay, we found that although a variety of cell cycle markers led to differing conclusions, the critical phenotype of arrest at G2-M was a shift in the population of cells from 2N to 4N DNA content. Distribution analysis of HCI data, in conjunction with the use of stringent cutoffs, defined significant changes in the populations of treated and untreated cells. As well as being an excellent marker for an arrested cell phenotype, these changes to DNA content facilitate the screening of large numbers of samples relatively quickly in a high-throughput setting.

Although improved assays decrease the time required to obtain results from a single experiment, the sampling used in the screen can itself be made more efficient. For HCI to become increasingly relevant as screening technology evolves, it is necessary to obtain a sampling that is statistically significant but not overly cumbersome. We determined that, in general, each field captured using HCI represents a random sampling of a population, that variability between replicate plates is negligible, and that quantitation of data from 600 cells is an ideal number to retain significant population sampling. Streamlining the discovery process simplifies the screening of large-compound and oligonucleotide libraries, facilitating efficient detection of novel phenotypes and targets.

Both ASOs and siRNAs are potential therapeutic agents, but their differential effects on gene knockdown remain poorly characterized. Although siRNA treatment has increasingly become the technique of choice for transient knockdown of a cellular target, ASOs have been in use significantly longer and have thus progressed further into clinical trials, with 1 drug already approved.[25] Stability and toxicity of ASOs have been largely ameliorated with 2 structural changes: phosphorothioate backbones and 2′-sugar modifications at the 5′ and 3′ ends. Phosphorothioate linkages lead to increased resistance to endonuclease digestion and better plasma protein binding, allowing for distribution to a variety of tissues after systemic dosing, whereas the addition of 2′-methoxyethyl-modified regions increase affinity for target mRNA, nuclease resistance, tissue uptake, and half-life. The ASOs used in this report were chimeric in nature, containing 2′ methoxyethyl-modified sugars in the 5′ and 3′ regions as well as a central section of deoxyribose. In the future, 1 or more of these molecule classes may be used in clinical combinatorial therapy, and it is therefore critical to understand how each of these molecules interacts with the machinery of the host cell to affect both target knockdown and phenotypic effects.

Using a variety of techniques, we determined that both siRNAs and ASOs knocked down a number of cellular factors significantly enough to perturb normal cell cycle function. Surprisingly, however, there was little correlation between the 2 forms of OMGS with the sole exception of AKT3, whose knockdown led to an increase in 4N DNA content, cyclin B expression, and pHH3 expression in both systems. Some of the disparity found between these 2 technologies may be due to differences in the target knockdown efficiency or the different mechanisms of action used by the 2 technologies and their attendant off-target effects. Interestingly, we have found that virally expressed short hairpin RNA (shRNA) against the same active targets indicates a better correlation with the siRNA data than with the ASO data (data not shown). This correlation may indicate that RNA-based knockdown methods are more robust or may be due to the similar mechanism of action used by shRNA and siRNA. The differential effects of ASOs and siRNAs may play a role as treatments advance through clinical trials. One OMGS treatment type or another may lead to an improved clinical outcome depending on the cellular target or the treatment used in conjunction with target knockdown.

ACKNOWLEDGMENTS

We thank Dr. Mark Uhlik, the members of the Stancato Laboratory, and the Lilly high-content imaging statistics and informatics team for helpful discussions and advice.

REFERENCES

1. Zamecnik PC, Stephenson ML: Inhibition of Rous sarcoma virus replication and cell transformation by a specific oligodeoxynucleotide. *Proc Natl Acad Sci U S A* 1978;75(1):280-284.
2. Jansen B, Wacheck V, Heere-Ress E, Schlagbauer-Wadl H, Hoeller C, Lucas T, et al: Chemosensitisation of malignant melanoma by BCL2 antisense therapy. *Lancet* 2000;356(9243):1728-1733.
3. Gewirtz AM: Oligonucleotide therapeutics: a step forward. *J Clin Oncol* 2000;18(9):1809-1811.
4. Monia BP, Lesnik EA, Gonzalez C, Lima WF, McGee D, Guinosso CJ, et al: Evaluation of 2′-modified oligonucleotides containing 2′-deoxy gaps as antisense inhibitors of gene expression. *J Biol Chem* 1993;268(19):14514-14522.
5. Braasch DA, Corey DR: Novel antisense and peptide nucleic acid strategies for controlling gene expression. *Biochemistry* 2002;41(14):4503-4510.
6. Davis AJ, Gelmon KA, Siu LL, Moore MJ, Britten CD, Mistry N, et al: Phase I and pharmacologic study of the human DNA methyltransferase antisense oligodeoxynucleotide MG98 given as a 21-day continuous infusion every 4 weeks. *Invest New Drugs* 2003;21(1):85-97.
7. Adjei AA, Dy GK, Erlichman C, Reid JM, Sloan JA, Pitot HC, et al: A phase I trial of ISIS 2503, an antisense inhibitor of H-ras, in combination with gemcitabine in patients with advanced cancer. *Clin Cancer Res* 2003;9(1):115-123.
8. Bartholomeusz C, Itamochi H, Yuan LX, Esteva FJ, Wood CG, Terakawa N, et al: Bcl-2 antisense oligonucleotide overcomes resistance to E1A gene therapy in a low HER2-expressing ovarian cancer xenograft model. *Cancer Res* 2005;65(18):8406-8413.
9. Marshall JL, Eisenberg SG, Johnson MD, Hanfelt J, Dorr FA, El-Ashry D, et al: A phase II trial of ISIS 3521 in patients with metastatic colorectal cancer. *Clin Colorectal Cancer* 2004;4(4):268-274.

10. Chi KN, Eisenhauer E, Fazli L, Jones EC, Goldenberg SL, Powers J, et al: A phase I pharmacokinetic and pharmacodynamic study of OGX-011, a 2′-methoxyethyl antisense oligonucleotide to clusterin, in patients with localized prostate cancer. *J Natl Cancer Inst* 2005;97(17):1287-1296.
11. Fire A, Xu S, Montgomery MK, Kostas SA, Driver SE, Mello CC: Potent and specific genetic interference by double-stranded RNA in *Caenorhabditis elegans*. *Nature* 1998;391(6669):806-811.
12. Bernstein E, Caudy AA, Hammond SM, Hannon GJ: Role for a bidentate ribonuclease in the initiation step of RNA interference. *Nature* 2001; 409(6818):363-366.
13. Hammond SM, Bernstein E, Beach D, Hannon GJ: An RNA-directed nuclease mediates post-transcriptional gene silencing in *Drosophila* cells. *Nature* 2000;404(6775):293-296.
14. Spee B, Jonkers MD, Arends B, Rutteman GR, Rothuizen J, Penning LC: Specific down-regulation of XIAP with RNA interference enhances the sensitivity of canine tumor cell-lines to TRAIL and doxorubicin. *Mol Cancer* 2006;5:34.
15. Nozawa H, Tadakuma T, Ono T, Sato M, Hiroi S, Masumoto K, et al: Small interfering RNA targeting epidermal growth factor receptor enhances chemosensitivity to cisplatin, 5-fluorouracil and docetaxel in head and neck squamous cell carcinoma. *Cancer Sci* 2006;97(10):1115-1124.
16. Barik S, Bitko V: Prospects of RNA interference therapy in respiratory viral diseases: update 2006. *Expert Opin Biol Ther* 2006;6(11):1151-1160.
17. Shen J, Samul R, Silva RL, Akiyama H, Liu H, Saishin Y, et al: Suppression of ocular neovascularization with siRNA targeting VEGF receptor 1. *Gene Ther* 2005;13(3):225-234.
18. Giuliano KA, Haskins JR, Taylor DL: Advances in high content screening for drug discovery. *Assay Drug Dev Technol* 2003;1(4):565-577.
19. Bennett CF, Cowsert LM. Antisense oligonucleotides as a tool for gene functionalization and target validation. *Biochim Biophys Acta* 1999; 1489(1):19-30.
20. Silverman BW. *Density Estimation for Statistics and Data Analysis*. London: Chapman & Hall/CRC, 1986.
21. Venables WN, Ripley BD: *Modern Applied Statistics with S*. New York: Springer, 2002.
22. Ghosh RN, Grove L, Lapets O: A quantitative cell-based high-content screening assay for the epidermal growth factor receptor-specific activation of mitogen-activated protein kinase. *Assay Drug Dev Technol* 2004; 2(5):473-481.
23. Montgomery DC: *Design and Analysis of Experiments*. New York: John Wiley & Sons, 1997.
24. Bilanges B, Stokoe D: Direct comparison of the specificity of gene silencing using antisense oligonucleotides and RNAi. *Biochem J* 2005; 388(pt 2):573-583.
25. Holmlund JT. Applying antisense technology: Affinitak and other antisense oligonucleotides in clinical development. *Ann N Y Acad Sci* 2003; 1002:244-251.

Address correspondence to:
Louis Stancato
Lilly Corporate Center
Bldg 98C, DC0434
Indianapolis, IN 46285

E-mail: l.stancato@lilly.com